Assessing the potential of PIV data to resolve hidden frequency scales

Maegan Vocke[1,*], Ralf Kapulla[2], Chris Morton[1]

1: McMaster University, Department of Mechanical Engineering, Hamilton, Canada
2: Paul Scherrer Institute, Villigen, Switzerland
*Corresponding author: vockem@mcmaster.ca

Keywords: PIV processing, Nyquist frequency, rapid distortion theory, convective velocity.

ABSTRACT

The present work investigates the performance of an advection-based flow reconstruction model to increase the temporal resolution of PIV measurements recorded in a turbulent, planar jet. Using a semi-Lagrangian technique in combination with Rapid Distortion Theory, a modified trajectory tracking procedure is implemented. The method introduces a specification for a two-dimensional convective velocity $\mathbf{U_c}$ based on the least squares minimization of the linearized advection equation, in contrast to the previously introduced one-dimensional mean velocity profile $\mathbf{U_m}$ outlined in Vocke et al. (2023). The new implementation is based on local flow measurements, making it well-suited towards streamwise heterogeneity and spatially developing flows. With this, the flow at some unknown time t_n can be estimated from the know flow measurements at the forward t_f and backward t_b time. Spectral analysis illustrates the model's proficiency in recovering spatiotemporal information far exceeding the Nyquist frequency, with spectral reconstruction errors of less than 5% for the most extreme case. It is demonstrated that the spectral content can be estimated at least two orders of magnitude beyond the sampling frequency of the original recording. Improved performance compared to alternative methods is demonstrated with only minor impact on computational time. This indicates the approach may be used as a tool for experimental researchers a) having no access to a high-speed PIV or b) with high-speed PIV to increase the spectral resolution even further.

1. Introduction

Particle image velocimetry (PIV) is a widespread experimental technique that provides instantaneous velocity field measurements. Despite PIV existing as the preferred measurement technique (Westerweel et al., 2013), the majority of PIV systems are limited in their ability to resolve the widespread temporal scales of most turbulent flows – particularly for challenging high Reynolds number flows. Accordingly, reconstruction of under-resolved spectral content remains an ongoing effort. We have previously addressed this problem through the development of an advection-based flow reconstruction technique using a semi-Lagrangian numerical scheme to increase the

temporal resolution of turbulent flow data (Vocke et al., 2023). The concepts outlined in Vocke et al. (2023) are extended in the present work to determine the amount, as well as the quality of spatiotemporal information that can be recovered beyond the Nyquist frequency through specification of a flow-dependent convective velocity. The performance of the temporal up-sampling method is verified using both numerical (DNS) and experimental (PIV) flow datasets recorded for a turbulent planar jet with sampling frequency f_s. We demonstrate that the spectral information of a PIV recording can be extended up to 100 times the Nyquist frequency.

The present investigation challenges the assumption that the spatiotemporal scales can be adequately modeled with a convective velocity equal to the local mean flow, as used in Taylor's hypothesis (Taylor, 1938). Assuming the turbulent structures maintain a frozen pattern as they are transported up to a certain distance downstream, the velocity fluctuations are generally described with $\mathbf{u}'(\mathbf{x}+\Delta\mathbf{x}, t+\Delta t) = \mathbf{u}'(\mathbf{x}+\Delta\mathbf{x}-\mathbf{U_m}\Delta t, t)$. The linear transformation using the mean velocity vector $\mathbf{U_m}$ violates the physical nature of the velocity fluctuations, as the space-time correlations along the characteristic lines $x - U_m t = const.$ will not decay with increasing Δt or Δx. While such approximation is appropriate for homogeneous flows, it becomes difficult to extend towards non-equilibruim type flows where the effects of mean shear, turbulence intensity, and viscous forces can be significant (Lin, 1953; Moin, 2009; Cheng et al., 2017; Mehrez et al., 2023; Jacobitz & Schneider, 2024). The question then arises, what defines an optimal convective velocity and when is it appropriate to assume that turbulent structures evolve according to the mean flow? Despite the relevance, there seems to be a lack of work regarding the characterization of convective velocities for different flow configurations (Álamo & Jiménez, 2009). Classically, this subject has been explored by authors such as Goldschmidt et al. (1981) and Wills (1964), who use correlation-based approaches to define both broadband and scale-dependent convective velocities. More recently, Álamo & Jiménez (2009) introduced a method based on a least-square minimization (LSM) of the linear advection equation to define the convective velocity of individual Fourier modes. This work was extended by Renard & Deck (2015) for application towards spatially developing flows. Utilizing the methods described by Álamo & Jiménez (2009) and Renard & Deck (2015), this work introduces a technique to increase the temporal resolution of turbulent flow measurements without any prior knowledge of the flow physics.

2. Methodology

The improved advection-based flow reconstruction model described in Vocke et al. (2023) was developed to overcome the limitations outlined by previous methods outlined in Scarano & Moore (2012) and Vamsi Krishna et al. (2020). Our own temporal up-sampling method was first developed using a benchmark data set of the direct numerical simulation (DNS) of a turbulent plane jet with $Re = 10,000$ and a non-dimensional sampling frequency of $f_s = 24.86$ (refer to Vocke et al. (2023) for further details). The concepts outlined in Vocke et al. (2023) are based on a one di-

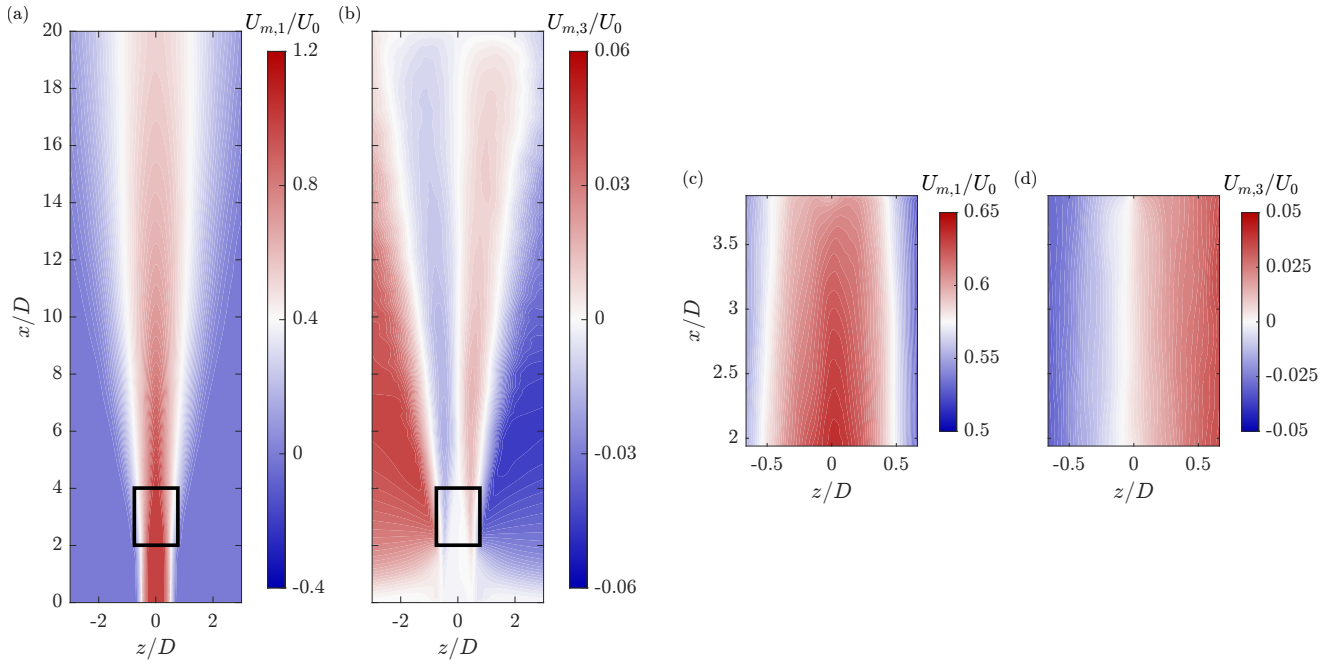

Figure 1. Comparison between the DNS (a-b) and PIV (c-d) FOV for the axial $U_{m,1}$ (a,c) and lateral $U_{m,3}$ (b,d) mean velocity components. The thick black boxes featured in (a-b) depict the difference in the FOV for the DNS and PIV datasets, wherein the DNS data depicts the entire development of the jet, while the PIV data is available only within the potential core ($2 < x/D < 4$ and $-0.7 < z/D < 0.7$).

mensional, uniformly sheared mean flow $\mathbf{U_m}$ approximation, while this is extended in the present work through the specification of a two-dimensional convective velocity $\mathbf{U_c}$ that may differ from the local mean flow. Following the work of Álamo & Jiménez (2009) and Renard & Deck (2015), a least-squares optimization is used to define the convective velocity $\mathbf{U_c}$ of all the scales. The method is additionally validated for use in experimental flow measurements. The PIV measurements comprises a turbulent planar jet with $Re = 3000$ generated from a contraction nozzle at the origin, sampled with $f_s = 10$ kHz, which corresponds to a non-dimensional frequency $f_s = 20.4$, and $N = 8000$. Further details regarding the experimental setup can be found in Neal et al. (2015). In contrast to the DNS dataset, the PIV recordings cover downstream distances from approximately $2D$ to $4D$. A comparison of the two benchmark datasets comparing the differences in field-of-view (FOV) is given in Figure 1. The performance of the advection method applied to the PIV measurements is evaluated through a sub-sampling procedure. Based on the original recordings with the sampling frequency f_s, a sub-sampling factor $S^* = f_s/f_n$ is used to obtain flow measurements with an artificially decreased sampling rate f_n. With this, the reconstructed velocity fields can be directly compared with the ground truth data.

Using Rapid Distortion Theory (RDT) in combination with a semi-Lagrangian numerical scheme, the temporal and spatial fluctuations are related by a convective velocity $\mathbf{U_c}$. Consequently, the

governing equation reduces to a quasilinear, non-homogeneous material derivative,

$$\frac{D\mathbf{u}'}{Dt} = \frac{\partial \mathbf{u}'}{\partial t} + (\mathbf{U_c} \cdot \nabla)\mathbf{u}' = -(\mathbf{u}' \cdot \nabla)\,\mathbf{U_c} \tag{1}$$

where $\mathbf{u}' = [u_1', 0, u_3']$, $\mathbf{U_c} = [U_{c,1}, 0, U_{c,3}]$, and $\nabla = [\partial_x, 0, \partial_z]$ represent the fluctuating velocities, convective velocities, and the gradient operator for a two-component flow, respectively. Using the spatiotemporal information from two successive flow measurements, the backward and forward evolution of the known data can be estimated. This is achieved using a semi-Lagrangian numerical technique, which describes the problem as a system of two ordinary differential equations. The equations are formulated in terms of a "forward" and "backward" estimate for known data with a temporal spacing of $f_s = (t_b - t_f)^{-1}$, resulting in two estimates for the flow at the unknown time t_n. These estimates are combined using a linear temporal weighting scheme wherein the intermediate results are weighted according to their proximity (in time) to the velocity fields from which they are derived,

$$\mathbf{u}'(\mathbf{x}, t_n) = \left(1 - \frac{n}{S^*}\right)\mathbf{u}_f'(\mathbf{x}, t_n) + \left(\frac{n}{S^*}\right)\mathbf{u}_b'(\mathbf{x}, t_n), \tag{2}$$

where $n \leq S^*$. Such weighting accounts for the decreasing reliability of the estimates as they progress towards the midpoint time, i.e., $n/S^* = 0.5$. Under the quasilinear approximation, the fluctuations are limited towards interactions with some convective velocity, which is generally assumed to be equal to the local mean velocity $\mathbf{U_m}$ (Goldschmidt et al., 1981). While such an assumption is valid for homogeneous flows, it becomes less accurate in regions subject to substantial mean shear, high turbulence intensity, and significant viscous effects (Hunt & Carruthers, 1990). This can lead to a distortion of the spatial scales, as well as negatively impact effects of amplitude modulation (Yang & Howland, 2018). Accordingly, it becomes important to specify a convective velocity that accurately describes the transport of turbulent fluctuations. Considering the simplest case of Taylor's hypothesis, which is generally valid for flows that are streamwise homogeneous (Taylor, 1938), the optimal streamwise convective velocity is determined through an inverse problem. This is achieved using a variational method to minimize the residual between the time evolution of the known flow data and its frozen wave approximation, $\mathbf{r} = \mathbf{u}(\mathbf{x}, t) - \mathbf{u}(\mathbf{x} + \Delta\mathbf{x}, t + \Delta\mathbf{x}/C)$. Here, C is the streamwise convective velocity of an ideal frozen wave and requires knowledge of the streamwise flow gradients ∂_x. This leads to 3 three approximations for the convective velocity depending on which variable is treated implicitly i.e., $(\mathbf{x}, t(\mathbf{x}))$ or $(\mathbf{x}(t), t)$, in the approximation. Importantly, all three definitions coincide for a truly frozen wave flow (Renard & Deck, 2015). The ideal value of C must be chosen such that it minimizes the square of the residual,

$$R_1(\mathbf{x}) = \frac{\overline{\left((1/C)\partial_t {u_1}' + \partial_x {u_1}'\right)^2}}{\overline{\left(\partial_x {u_1}'\right)^2}} \tag{3}$$

The values of C can be interpreted as some constant factor that best relates the spatial and temporal derivatives. Minimizing Eqn. (3) over C leads to the following definition for the convective

velocity,

$$U_{c,1}(\mathbf{x}) = -\frac{\overline{(\partial_t u_1{}')^2}}{\overline{(\partial_t u_1{}' \partial_x u_1{}')}}. \tag{4}$$

This leads to the definition of the convective velocity based on LSM. Notably, the calculation of $U_{c,1}$ requires only the stationary time averages of local signals and their derivatives. For flow measurements with two or more velocity components, $U_{c,1}$ can be similarly estimated from either component depending on the constraints placed on the parameter C. Additionally, the optimal streamwise space-time correlation coefficient γ_1 is defined as,

$$\gamma_{c,1}(\mathbf{x}) = \sqrt{1 - R_1(\mathbf{x})} = \frac{\overline{(\partial_t u_1{}' \partial_x u_1{}')}}{\sqrt{\overline{(\partial_t u_1{}')^2}}\sqrt{\overline{(\partial_x u_1{}')^2}}}, \tag{5}$$

where $0 \leq \gamma_{c,1} \leq 1$. For the case of ideal convection, the spatial and temporal derivatives are perfectly correlated, i.e., $\gamma_{c,1} = 1$. A value of $\gamma_{c,1} < 1$ provides a measure of the degree of decay or deformation that occurs as the turbulent structures evolve downstream. Thus, the method serves to validate when the simplified numerical approach is justified by identifying regions where $U_{c,1} \approx U_{m,1}$. The present work obtains the streamwise component of the convective velocity vector $\mathbf{U_c}$ by computing the least-squares solution to the one-dimensional linear advection equation. In contrast, the lateral component of $\mathbf{U_c}$ is simply assumed to be equal to the lateral component of the mean velocity vector, $U_{c,3} = U_{m,3}$. In principle, a LSM approximation to $U_{c,3}$ could be obtained by consider the contribution of lateral gradients ∂_z. The convective velocity can be similarly estimated from the normalized cross correlation function ρ_{ij}, which is numerically equivalent to the LSM method. Defining the normalized correlation of two signals separated by spatial distance $\Delta\mathbf{x}$, where the upstream signal lags by time delay Δt, results in

$$\rho_{ij}(\mathbf{x} + \Delta\mathbf{x}, t + \Delta t) = \frac{\overline{u_i'(\mathbf{x}, t) u_j'(\mathbf{x} + \Delta\mathbf{x}, t + \Delta t)}}{\sqrt{\overline{u_i'}(\mathbf{x}, t)^2}\sqrt{\overline{u_j'}(\mathbf{x} + \Delta\mathbf{x}, t + \Delta t)^2}}. \tag{6}$$

The convective velocity relates the temporal scales to the various spatial scales within a flow, $U_c = \Delta x / \Delta t$. The parameters for Δx and Δt can be defined by maximizing over the time lag Δt for a given spatial separation Δx, yielding $f(\Delta x) = \Delta t_{max}$. Physically, this definition of U_c can be related to the micro-scales in a convective reference frame ($x_c = x - U_c t, t$), thus guaranteeing the slowest spatial decay of the correlation (Renard & Deck, 2015).

3. Results and Discussion

The results are presented and discussed as follows. Firstly, a brief analysis characterizing both the streamwise convective velocity estimations $U_{c,1}$ and the mean velocity fields $U_{m,1}$ of the DNS and experimental jet data is presented. The next section provides qualitative and quantitative assessment of the temporal reconstruction model.

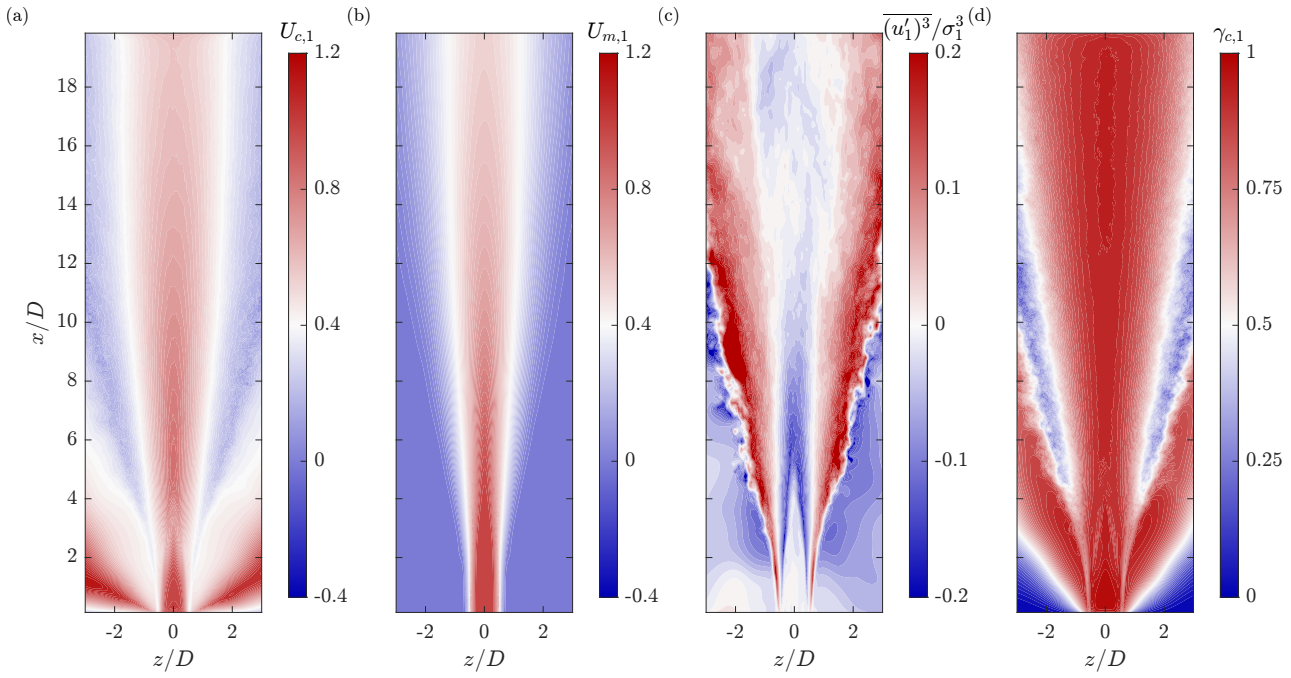

Figure 2. Comparison between the local (a) convective velocity and (b) mean velocity, as well as (c) the spatial distribution of the normalized velocity skewness and (d) the optimal correlation coefficient γ_c for the DNS data.

3.1. Convective velocity estimation

A comparison between the LSM-based convective velocity $U_{c,1}$ and streamwise component of the mean velocity $U_{m,1}$ is displayed in Figure 2 (a) and (b). Towards the high speed side of the mixing layer, between $2 < x/D < 4$, the convective velocity is generally lower than the mean velocity. In contrast, near the lateral edges the convective velocity is generally greater than the mean velocity. Additional lateral differences are noted towards the inlet of the domain, for $x/D < 2$. In these regions, the stagnant flow is not yet significantly influenced by the jet, thus, predicting the convective velocity is both difficult and essentially irrelevant in this region. In the fully developed region ($x/D > 10$), $U_{c,1}/U_{c,1} \approx 1$ towards the jet centerline, however, the $U_{c,1}$ towards lateral edges is consistently faster. The optimal correlation coefficient displayed in Figure 2 (d) is $\gamma_{c,1} \approx 1$ throughout the majority of the spatial domain, however, the value drops dramatically along the developing shear layers and towards the region of stagnant flow as previously described. Importantly, the lateral regions where the optimal convective velocity is unity coincide with regions where $U_{c,1} \neq U_{m,1}$. Analyzing the spatial and temporal derivatives, $\gamma_{c,1} \ll 1$ when the variation of these derivatives in one direction (i.e., either space or time) is much faster than the other (observed for $x/D > 4$), or alternatively when there is no preferential direction between the spatial and temporal derivatives (observed for $x/D < 4$). This is not the case along the jet centreline. Here, the optimal correlation coefficient is approximately unity, yet, significant deviation between $U_{c,1}$ and $U_{m,1}$ can be observed. This implies that something other than the linear dependency of the spatial and tem-

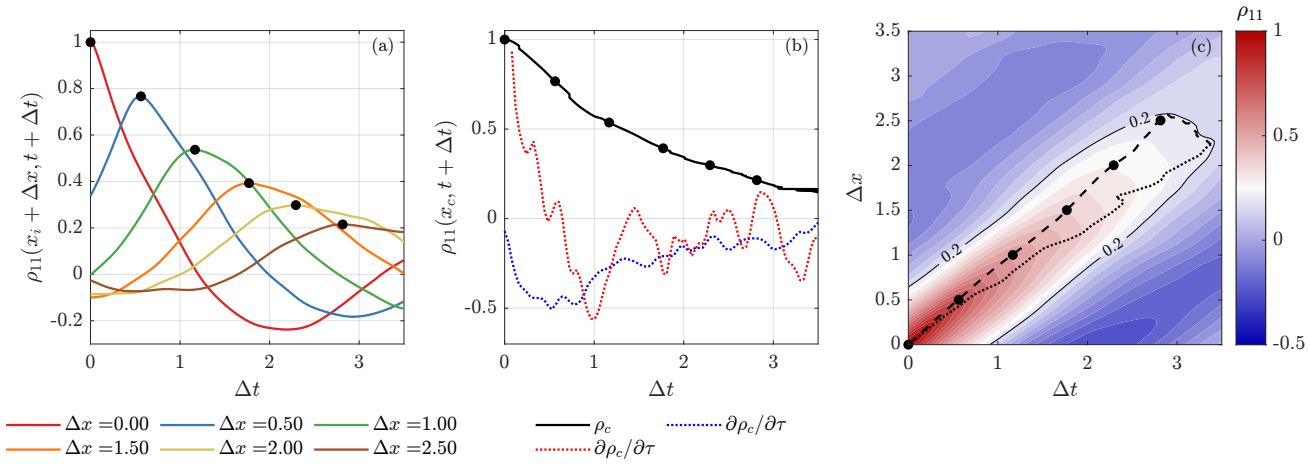

Figure 3. (a) Series of cross correlation measurements of the DNS jet for the u-component of velocity with the reference point $x_i = 5.0$. Each curve represents a different downstream separation. (b) Same series of cross correlation curves in a convective frame ($x_c = x - U_c t, t$) (c) Corresponding space-time correlation of the DNS jet. The solid black line corresponds to the limit for the significance of correlation, σ_N.

poral derivatives is causing the deviation. One possible explanation derives from the skewness of the velocity fluctuations, displayed in Figure 2 (c). Skewness is a third-order moment that indicates the degree of asymmetry within a probability distribution. The LSM and correlation-based methods consider the square of the signal, thus, are strongly influenced by large amplitude fluctuations. Physically, skewness is an important parameter in understanding turbulent kinetic energy, wherein the gradient of $\overline{u_j' u_j' u_i'}$ represents the rate at which Reynolds stresses are transported by the turbulent fluctuations. Observing Figure 2 (c), the skewness is positive along the developing shear layer, with distinct negative regions outlining the potential core. Such behaviour is characteristic of multi-scale entrainment phenomena wherein the ambient fluid is engulfed towards the jet centreline due to shear across a turbulent/non-turbulent interface. Generally, the skewness decays towards zero as the flow becomes fully developed. Comparing Figure 2 (a), (b), and (c), there seems to be a qualitative agreement between regions of non-zero skewness to regions where where $U_{c,1} \neq U_{m,1}$.

The axial space-time correlations of the DNS data computed with respect to the reference point $\mathbf{x}/D = (5.0, 0)$ are displayed in Figure 3 (a)-(c). As mentioned in Section 2, the convective velocity $U_{c,1}$ can be determined from the time delay which maximizes the correlation coefficient for a given spatial separation, or alternatively by considering the spatial separation that maximizes the correlation for a given time delay. A broadband estimate of $U_{c,1}$ is obtained by considering the *envelope* of significant correlations as estimated from white noise. For correlations based on N samples, the variability observed across multiple white noise correlations forms the basis for the statistical significance threshold, $\sigma_N = 0.2$ for the present dataset. As with the LSM method, these definitions should coincide if there is a significant linear dependence between space and time. Thus, Taylor's hypothesis can be applied in regions where $\partial_t \, \rho_{11} = \partial_x \, \rho_{11}$. The local maximum values of

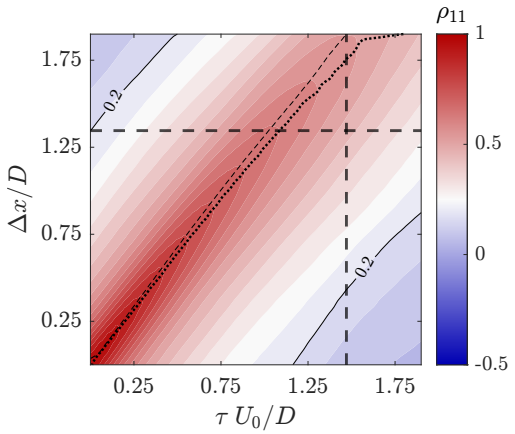

Figure 4. Space-time correlation of the PIV jet for the u-component of velocity along the centreline at $x/D = 2.0$. The thin dashed and dotted lines represent the maximum of the correlations with respect to Δt and Δx respectively. The vertical and horizontal black dashed lines represent the time lag and spatial separation that correspond to the limit for the significance of correlation, σ_N.

the correlations based on a constant time delay (thin dashed line) and a constant spatial separation (thin dotted line) are displayed in Figure 3 (c). For $\Delta t > 0.5$ we observe a deviation in slope of the maximum correlation. This is to be expected within the developmental zone, where one is likely to find significant flow decorrelation induced by the combined effects of convection, mean flow shear, and the random motion associated with the interactions between various flow scales. Considering the PIV data, Figure 4 displays the axial space-time correlations computed using a reference point $\mathbf{x}/D = (2.0, 0)$ (i.e., within the potential core). The local peak values indicate that $\Delta x/\Delta t$ remains approximately constant within the significance region bounded by σ_N, thus, Taylor's hypothesis is a valid simplification for this region of the flow.

3.2. Evaluation of the temporal reconstruction model

The performance of the temporal reconstruction model is evaluated through a direct comparison of the power spectral density $\Phi_{11}/\overline{u_1' u_1'}$ as a function of the normalized frequency fD/U_0 for the axial velocity u to the reference PIV data in Figure 5(c). As $U_{c,1} \approx U_{m,1}$ for the reference PIV data, the spectra computed with respect to $U_{m,1}$ is not shown. The performance of the model applied to the reference DNS data (Vocke et al., 2023) is similarly displayed for calculations based on $U_{c,1}$ and the two-dimensional $U_{m,1}$ (refer to Figure 5 (a) and (b), respectively). In general, advection based on $U_{m,1}$ fails to capture the fundamental frequency of the jet instability due to the relatively large velocity gradients surrounding the jet core for $x/D < 4$. For both the flow cases based on $U_{c,1}$ (Figure 5(a) and (c)), a slight increase in the energy content is observed for frequencies below the Nyquist frequency f_N of the under sampled data. The most notable differences appear in the higher frequency range of the spectra, where the reconstructed PIV data demonstrates a stronger capability to capture the spectral end behavior compared to the reconstructed DNS data. It is pos-

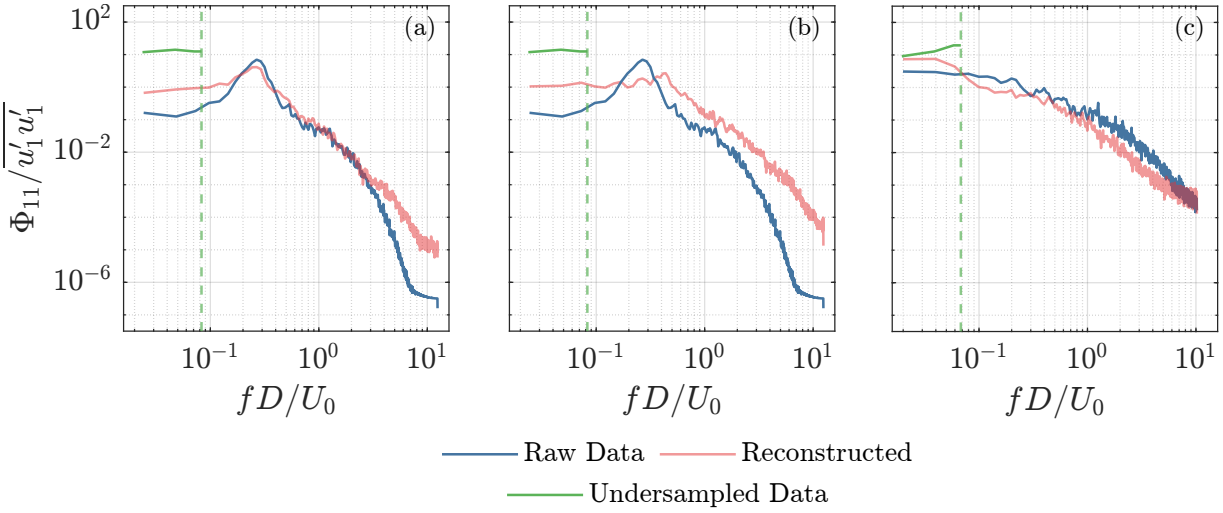

Figure 5. Comparison of the raw, under sampled, and reconstructed (a) DNS spectrum computed with the LSM-based $\mathbf{U_c}$ (b) DNS spectrum computed with the two-dimensional $\mathbf{U_m}$, and (c) PIV spectrum computed with $\mathbf{U_c}$ for the u-component of the velocity field. The green dashed lines represent the Nyquist frequency f_N of the under-sampled data set. The spectra are extracted along the jet centreline at $x/D = 3.0$ and presented in a log-log scale.

sible that some deviation stems from the difference in Reynolds numbers for the two data sets, with $Re_{DNS} = 10,000$ and $Re_{PIV} = 3000$. Thus, the turbulence of the PIV data set is still in its early stages of development at this location in the domain. It is important to note however that the range of resolvable frequencies for the PIV measurements is limited by the available spatial resolution. The maximum resolvable frequency is often estimated by considering the ratio of some bulk convective velocity and smallest resolved length scale, $f_{max} = U_0/\delta$ (Schneiders et al., 2018). If δ is assumed from the interrogation window size, this results in $f_{max}D/U_0 \approx 7$, giving reasonable evidence that the majority of the PIV spectrum has been resolved. This is further verified by considering the comparison of the PIV recordings as outlined in Neal et al. (2015), which were obtained using a high-dynamic range (HDR) system, to the equivalent hot-wire (HW) measurements in the fully-develop turbulence region. Neal et al. (2015) showed that the PIV-HDR measurements exhibit slight deviation from the HW measurements in the form of high-frequency roll-up. Recall that the FOV for the PIV data is smaller than that of the original DNS time series. To ensure a proper comparison of the results, the FOV for the DNS data was truncated to cover the same downstream distance as the PIV measurements before applying the upsampling algorithm.

To quantify the error bounds of our method we use two metrics, the *time-varying reconstructed errors*, $\epsilon_i(t^*)$, and the *spectral reconstruction errors*, $E_{ii}(\mathbf{x}, f)$. The time-varying reconstructed errors displayed in Figure 6 are defined with the following equation,

$$\epsilon_i(t^*) = \frac{100}{U_0}\left[\frac{1}{N_x}\frac{1}{N_z}\sum_{a=1}^{N_x}\sum_{b=1}^{N_z}[\widetilde{u_i}'(x_a, z_b, t^*) - u_i'(x_a, z_b, t^*)]^2\right]^{1/2} \tag{7}$$

where u_i' and $\widetilde{u_i}'$ represent the reference and reconstructed velocity data, respectively. In general,

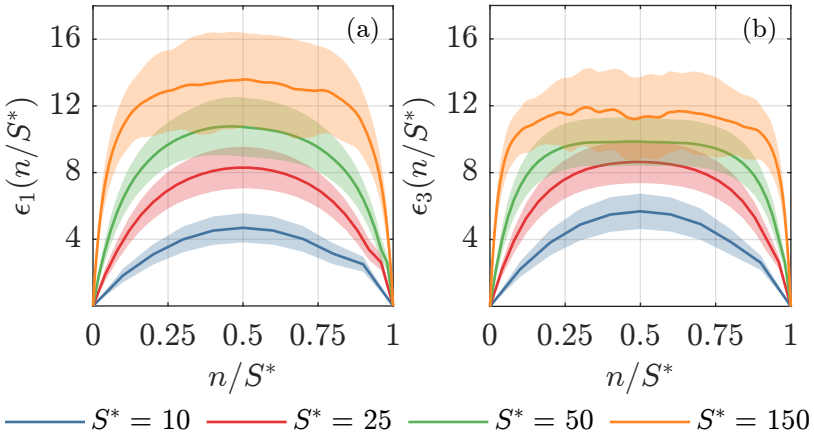

Figure 6. Temporal reconstruction error for the reference PIV data as a percent error according to Eqn. 7 for the (a) u-component and (b) w-component of the flow. The error uncertainty is displayed with the transparent bands indicating one standard deviation from the mean.

there exists a slightly greater uncertainty throughout the majority of the up-sampling period for the case of $S^* = 150$, likely due to the limited number of samples (54) used to compute the statistics. A plateau of the errors occurs for both velocity components towards the midpoint time $n/S^* = 0.5$, which is expected due to the linear temporal weighting scheme. The plateau for the u_1' velocity component develops much faster for the case with $S^* = 150$ compared with the less extreme cases, indicating $S^* = 150$ corresponds to the upper limit for what can be recovered from the experimental dataset. Additionally, the plateau of the error occurs faster for the lateral velocity component u_3'. This could be related to the use of $U_{m,3}$ instead of an optimized lateral convective velocity $U_{c,3}$.

The spectral reconstruction error in the form of a pre-multiplied energy difference is used to asses the model's ability to recover spatiotemporal information, and is calculated according,

$$E_{ii}(\mathbf{x}, f) = 100\,\frac{fU_0}{D}\,\frac{\widetilde{\Phi}_{ii}(\mathbf{x}, f) - \Phi_{ii}(\mathbf{x}, f)}{\langle u_i'(\mathbf{x}, t)\, u_i'(\mathbf{x}, t)\rangle}, \tag{8}$$

where $\widetilde{\Phi}_{ii}(\mathbf{x}, f)$ and $\Phi_{ii}(\mathbf{x}, f)$ represent the up-sampled and reference spectra, respectively. The spectral reconstruction errors extracted along the jet centreline for the cases $S^* = 50$ and 150 are displayed for the u' and w' components of velocity in Figure 7. Similar trends are observed for both sub-sampling factors and velocity components, with a distinct energy gain marking the boundary along the Nyquist frequency of the under sampled data set, and a consistent small energy loss moving towards the high frequencies. The numerical scheme uses the known forward and backward flow measurements as the initial conditions for each estimate of the velocity field at t_n (i.e., the flow at t_n is never used as the initial conditions for the time t_{n+1}). It is possible that the energy gain indicates the limitations of the proposed time-marching scheme, as the the velocity fields at times t_f and t_b leave their imprint on each successive estimate.

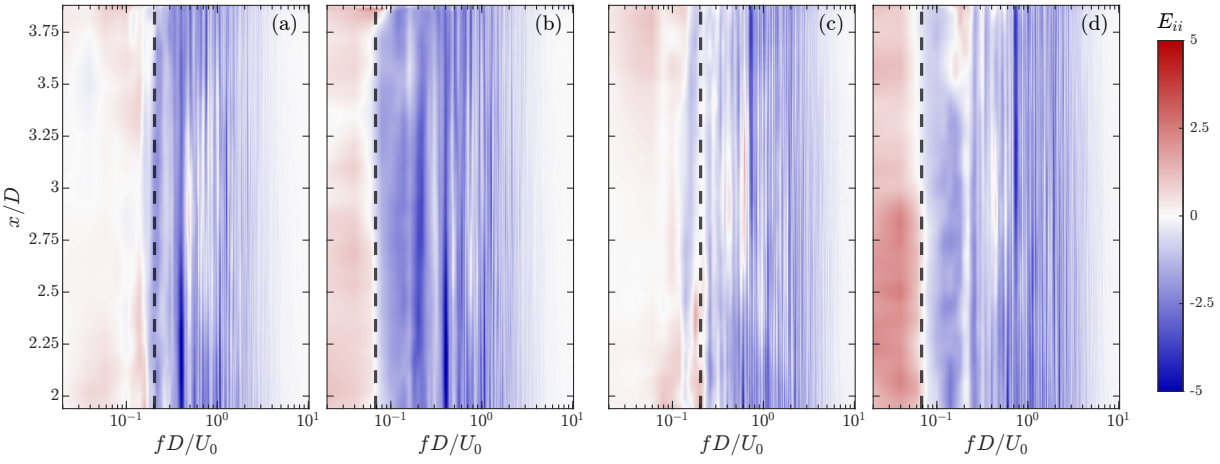

Figure 7. Planar distribution of the spectral reconstruction error based on the reference PIV data for the (a,b) u-component and (c,d) w-component of velocity along the jet centreline, for the sub-sampling factor (a,c) $S^* = 50$ and (b,d) $S^* = 150$. The black dashed lines represent the Nyquist frequency f_N of the under-sampled data set.

4. Conclusions

This study extends upon the concepts outlined in Vocke et al. (2023) to assess what spatiotemporal data can be recovered from an experimental PIV data set. Using both a benchmark DNS and PIV dataset of a turbulent planar jet, the convective velocity of all scales is estimated using an LSM-based techniques. An important feature of this technique is the ability to asses the linear dependency between space and time – thus providing a metric to asses the validity of Taylor's Hypothesis through an optimal correlation coefficient. While this metric is reliable in the fully-developed region of the flow, it fails to predict deviations between U_m and U_c towards the potential core and developmental region. Instead, the skewness of the fluctuations is proposed as a possible indicator of such deviations. This convective velocity estimation is used in combination with a semi-Lagrangian numerical technique to recover spectral information well-beyond the Nyquist limit. Importantly, the method requires no *a priori* knowledge of the flow physics and is well suited towards non-equilibrium flows with significant developmental regions. The evaluation of the model applied to experimental turbulent planar jet measurements at $Re = 3000$ highlights its potential to capture important trends in the spectrum, especially in the inertial sub-range towards viscous dissipation, demonstrating promise for turbulent flow analysis. The quantitative performance of the flow reconstruction is investigated according the time-varying and spectral reconstruction errors, where the reported errors were less than 15% and 5%, respectively. These preliminary findings offer a valuable framework for future investigations which aim to refine the model's accuracy, particularly in regions where the simplified assumptions of Taylor's hypothesis and RDT require further refinement. Future work includes application of the model to different flow configurations and Reynolds numbers to further verify the method's generality.

Acknowledgements

We would like to graciously thank Dr. Andrea Sciacchitano of TUDelft for enabling this work by providing the experimental data set. We extend further gratitude towards Dr. Markus Klein for providing the high-quality benchmark DNS data. Additionally, the first approach – leading to this publication – outlining the capabilities of PIV as documented in Vocke et al. (2023) would not have been possible without the financial support in 2022 through the NEA/NEST (Nuclear Education, Skills and Technology) framework. We thank Andreas Pautz as the Chair of the NEST management board for his continuous support.

References

Cheng, Y., Sayde, C., Li, Q., Basara, J., Selker, J., Tanner, E., & Gentine, P. (2017). Failure of Taylor's hypothesis in the atmospheric surface layer and its correction for eddy-covariance measurements. *Geophysical Research Letters*, *44*(9), 4287–4295. doi: 10.1002/2017GL073499

Goldschmidt, V. W., Young, M. F., & Ott, E. S. (1981). Turbulent convective velocities (broadband and wavenumber dependent) in a plane jet. *Journal of Fluid Mechanics*, *105*, 327–345. doi: 10.1017/S0022112081003236

Hunt, J. C. R., & Carruthers, D. J. (1990). Rapid distortion theory and the 'problems' of turbulence. *Journal of Fluid Mechanics*, *212*, 497–532. doi: 10.1017/S0022112090002075

Jacobitz, F. G., & Schneider, K. (2024). Revisiting Taylor's hypothesis in homogeneous turbulent shear flow. *Physical Review Fluids*, *9*(4), 044602. doi: 10.1103/PhysRevFluids.9.044602

Lin, C. C. (1953). On Taylor's hypothesis and the acceleration terms in the Navier-Stokes equation. *Quarterly of Applied Mathematics*, *10*(4), 295–306. doi: 10.1090/qam/51649

Mehrez, A., Yamamoto, Y., & Tsuji, Y. (2023). Taylor's frozen hypothesis of the pressure fluctuations in turbulent channel flow at high Reynolds numbers. *Journal of Fluid Mechanics*, *972*, A15. doi: 10.1017/jfm.2023.692

Moin, P. (2009). Revisiting Taylor's hypothesis. *Journal of Fluid Mechanics*, *640*, 1–4. doi: 10.1017/S0022112009992126

Neal, D. R., Sciacchitano, A., Smith, B. L., & Scarano, F. (2015). Collaborative framework for PIV uncertainty quantification: the experimental database. *Measurement Science and Technology*, *26*(7), 074003. doi: 10.1088/0957-0233/26/7/074003

Renard, N., & Deck, S. (2015). On the scale-dependent turbulent convection velocity in a spatially developing flat plate turbulent boundary layer at Reynolds number. *Journal of Fluid Mechanics*, *775*, 105–148. doi: 10.1017/jfm.2015.290

Scarano, F., & Moore, P. (2012). An advection-based model to increase the temporal resolution of PIV time series. *Experiments in Fluids*, *52*(4), 919–933. doi: 10.1007/s00348-011-1158-3

Schneiders, J. F. G., Avallone, F., Pröbsting, S., Ragni, D., & Scarano, F. (2018). Pressure spectra from single-snapshot tomographic PIV. *Experiments in Fluids*, *59*(3), 57. doi: 10.1007/s00348-018-2507-2

Taylor, G. I. (1938). The Spectrum of Turbulence. *Proceedings of the Royal Society of London. Series A, Mathematical and Physical Sciences*, *164*(919), 476–490.

Vamsi Krishna, C., Wang, M., Hemati, M. S., & Luhar, M. (2020). Reconstructing the time evolution of wall-bounded turbulent flows from non-time-resolved PIV measurements. *Physical Review Fluids*, *5*(5), 054604. doi: 10.1103/PhysRevFluids.5.054604

Vocke, M., Kapulla, R., Morton, C., Klein, M., & Martinuzzi, R. J. (2023). Advection-based temporal reconstruction technique for turbulent velocity fields. *Physics of Fluids*, *35*(1), 015123. doi: 10.1063/5.0129564

Westerweel, J., Elsinga, G. E., & Adrian, R. J. (2013). Particle Image Velocimetry for Complex and Turbulent Flows. *Annual Review of Fluid Mechanics*, *45*(Volume 45, 2013), 409–436. doi: 10.1146/annurev-fluid-120710-101204

Wills, J. a. B. (1964). On convection velocities in turbulent shear flows. *Journal of Fluid Mechanics*, *20*(3), 417–432. doi: 10.1017/S002211206400132X

Yang, X. I. A., & Howland, M. F. (2018). Implication of Taylor's hypothesis on measuring flow modulation. *Journal of Fluid Mechanics*, *836*, 222–237. doi: 10.1017/jfm.2017.803

Álamo, J. C. D., & Jiménez, J. (2009). Estimation of turbulent convection velocities and corrections to Taylor's approximation. *Journal of Fluid Mechanics*, *640*, 5–26. doi: 10.1017/S0022112009991029